



Optimization of thermal and flow characteristics of plate heat exchanger with variable structure parameter

Chao Yu¹ · Xiangyao Xue¹ · Kui Shi¹ · Mingzhen Shao¹

Received: 23 May 2021 / Accepted: 21 June 2022 / Published online: 2 August 2022
© Akadémiai Kiadó, Budapest, Hungary 2022

Abstract

The plate heat exchanger is an efficient and compact heat exchanger, which has the advantages of high heat transfer coefficient and compact structure compared with other heat exchangers. The CFD simulation, radial basis function and multi-objective optimization are used to determine the optimal plate heat exchanger structure. Because there are two conflicting objectives that heat transfer coefficient j and friction coefficient f , the multi-objective genetic algorithm (MOGA) is selected, and the approximation model is obtained with radial basis function (RBF). The optimization results showed that heat transfer factor j increased by 26.9%, while friction factor f decreased by 25%, suggesting enhanced convective heat transfer and significantly reduced flow resistance. In each field of the longitudinal section, the optimized model velocity field increases by 0.01%, the pressure field decreases by 40%, and the temperature decreases by 2.5%. Then, the internal flow field is qualitatively compared from the aspects of field synergy angles and verified the rational optimization results. In this paper, multi-objective optimization method and CFD simulation are used to predict the structure of heat exchanger, rather than through the expensive and time-consuming experiment. This optimization method can save the design expense and time for the designer to design the plate structure that meets the requirements. This kind of multi-objective optimization design combined with simulation can provide a precise design method for designers.

Keywords Plate heat exchanger · CFD simulation · Radial basis function · Multi-objective optimization

Abbreviations

δ	Wavy plate height [mm]
c_i	Center of clustering
λ	Wavy plate angle [°]
∇T	Temperature gradient [°C m ⁻¹]
β	Wavy plate spacing [mm]
∇p	Pressure gradient [Pa m ⁻¹]
t	Wavy plate thickness [mm]
∇u	Velocity gradient [s ⁻¹]
j	Heat transfer factor
f	Friction factor
k	Heat transfer coefficient [W m ⁻² ·K ⁻¹]
Re	Reynolds number
T	Temperature [°C]
Pr	Prandtl number
D	Hydraulic diameter [m]
Nu	Nusselt number

ΔP	Pressure difference [Pa]
m	Mass flow [kg s ⁻¹]
ρ	Density [kg m ⁻³]
c_p	Constant-pressure specific heat [J kg ⁻¹ °C ⁻¹]
μ	Dynamic viscosity [N sm ⁻²]
w	Mass
λ_t	Thermal conductivity [W m ⁻¹ °C ⁻¹]
n	Number of sample
σ	Variance of basis function
u_i, v_j, w_k	Velocity component in coordinate system [m s ⁻¹]

Introduction

As a kind of compact heat exchangers, plate heat exchangers have high efficiency and low mass, widespread applications in aerospace, automobile and power machinery. Plate heat exchanger used for oil can significantly improve the service life and efficiency of equipment. Therefore, improving the efficiency of heat exchanger has important engineering significance. The optimization of internal flow field of heat exchanger is mainly to improve the performance of heat

✉ Chao Yu
yuchao@ciomp.ac.cn

¹ Changchun Institute of Optics, Fine Mechanics and Physics, Chinese Academy of Sciences, Changchun 130033, China

exchanger optimally in a certain size range [1–4]. Through the experimental study of gully type of plate heat exchanger, the influence of gully on heat transfer performance is analyzed and determined, which provides the basis for the selection of plate style [5–9].

On the basis of the experiment, the numerical simulation method is used to study the plate heat exchanger of different structure in detail. Through simulation analysis, the flow state of different inlet and outlet shapes of plate heat exchanger and the structural characteristics of plate are studied. The influence of different factors on fluid flow and heat transfer is analyzed [10–20]. Ranganayakulu Chennu [21] studied the single-phase steady-state heat transfer and pressure drop of passages and fins of compact heat exchangers. Qinguo Zhang [22] analyzed the heat transfer characteristics of the plate-fin heat exchanger in the cold air heating system of a PEMFC engine. Al-Obaidi A R [23–31] studied circular corrugated pipes of different structures and obtained corresponding flow field changes. Yuan Zhicheng [32] studied shape optimization and heat transfer analysis of welded plate-fin (WPF) heat exchanger with straight gas channels and corrugated water channels. Byung Hoon Shon [33] experimentally studied the characteristics of condensation heat transfer and frictional pressure drop. Jian Wen [34] numerically studied the comprehensive performance of serrated fin in plate-fin heat exchangers by using the analytical methods based on fluid structural interactions.

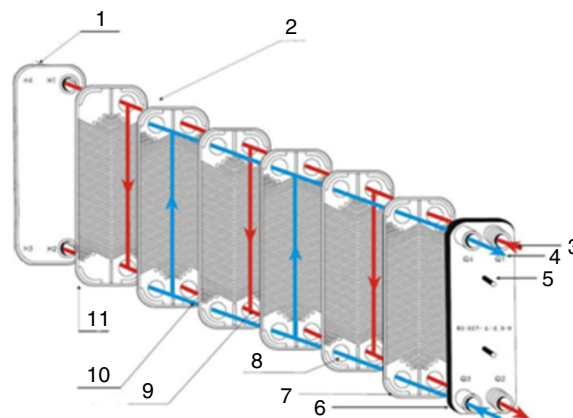
The new fluid media has attracted the attention of researchers gradually. A large number of studies on the novel nanoflow and the results confirmed that nanoflow would become a new direction for enhancing convective heat transfer [35–38]. Wen Jian [39] established a mathematical model for the influence of flow maldistribution in multi-channel heat exchanger. At the same time, computational fluid dynamics (CFD) technique was used to establish the heat exchanger model, considering the influence of the main channel, the collector and the distributor on the fluid distribution in the heat exchanger core. Shah Z, Shutaywi M and Sheikholeslami M [40,41–43] studied nanoflow in porous closed bodies. The influence of nanoflow on flow and heat distribution is obtained by numerical simulation.

This paper provides a method of high-performance heat exchanger structure size which can be quickly obtained for designers according to the characteristic design requirements. We select four main parameters of wavy plate and carry out MOGA to enhance the performance of plate heat exchangers. The wavy height δ , wavy pitch λ , wavy angle β and plate thickness t were defined as the parameters variable to obtain the heat transfer factor j and friction factor f . Then, the maximum j and minimum f were chosen as the standards of wavy plate heat exchangers. The optimal structural parameters of heat exchanger are obtained by radial basis function and genetic algorithm. Finally,

comparison with the original model verifies the rationality of optimization. This paper combines MOGA, RBF and CFD to find the optimal size structure within the scope of design, which provides guidance for designers to save design time and cost.

Structure parameters of WPFs heat exchangers

In the engineering field, there are many kinds of plate radiators, but their working principle is basically the same. As shown in Fig. 1, the hot fluid 3 enters the hot fluid passage 9 formed by the two plates through the corner hole 8 and flows through the channels formed by the upper and lower corrugated plates. Because of the flow passage is tortuous and complex, strong turbulence will be formed when the fluid flows. Hot and cold fluids flow in opposite directions on both sides of the plate, and heat transfer through the plate is more sufficient. Therefore, the required heat transfer effect can be achieved. So the requirement of higher heat dissipation efficiency is put forward for wavy plate in reasonable size range. In order to obtain the optimal heat dissipation structure size, this research was carried out. The simplified three-dimensional model in this research is shown in Fig. 2. The δ is wavy plate length. The λ is wavy plate spacing. The β is wavy plate angle. The t is wavy plate thickness. In the experiment of this plate heat exchanger, the engine oil and water flow through the two side of plate which made of aluminum, respectively.



1—Floor; 2—Flow of plates; 3—Hot fluid; 4—Cold fluid; 5—Bolt; 6—Cover plate; 7—First plate; 8—The Angle of hole; 9—Hot fluid channel; 10—Cold fluid channel; 11—Last plate;

Fig. 1 Plate heat exchanger structure. 1—Floor; 2—flow of plates; 3—hot fluid; 4—cold fluid; 5—bolt; 6—cover plate; 7—first plate; 8—angle of hole; 9—hot fluid channel; 10—cold fluid channel; 11—last plate

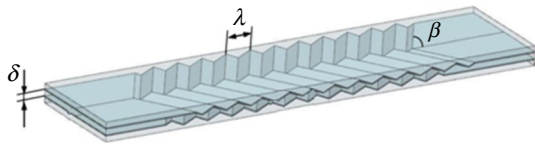


Fig. 2 Plate heat exchanger model

Numerical simulation of wavy plate heat exchangers

Mathematical model

The CFD uses the fast computing power of computers to obtain approximate solutions of fluid governing equations [42–45]. Because the coolant flow through the wavy plate channel is a complex thermal flow process, CFD flow field is selected to solve it. Through solving the control equation, CFD obtains the distribution characteristics of flow field in the channel.

The continuity and momentum equations of incompressible flow are as follows [47]:

$$\frac{\partial \rho}{\partial t} + \frac{\partial(\rho u_i)}{\partial x_i} = 0$$

$$\frac{\partial(\rho u_i)}{\partial t} + \frac{\partial(\rho u_i u_j)}{\partial x_j} = -\frac{\partial p}{\partial x_i} + \frac{\partial}{\partial x_j} \left(\mu \frac{\partial u_i}{\partial x_j} \right) + \frac{\partial \tau_{ij}}{\partial x_j} \tag{1}$$

where the Reynolds stress τ_{ij} is:

$$\tau_{ij} = -\overline{\rho u_i u_j} \tag{2}$$

The most widely used turbulence model is the standard $k-\epsilon$ model. The model is based on the kinetic energy k equation, and then, an equation of turbulent dissipation rate ϵ is introduced. The ϵ is defined as:

$$\epsilon = \frac{\mu}{\rho} \overline{\left(\frac{\partial u'_i}{\partial x_k} \right) \left(\frac{\partial u'_i}{\partial x_k} \right)} \tag{3}$$

The turbulent viscosity can be expressed as a function of k and ϵ :

$$\mu_t = \rho C_\mu \frac{k^2}{\epsilon} \tag{4}$$

Therefore, the transport equation of the standard $k-\epsilon$ model is [21]:

$$\frac{\partial(\rho k)}{\partial t} + \frac{\partial(\rho k u_i)}{\partial x_i} = \frac{\partial}{\partial x_j} \left[\left(\mu + \frac{\mu_t}{\sigma_k} \right) \frac{\partial k}{\partial x_j} \right] + G_k + G_b - \rho \epsilon - Y_M + S_k \tag{5}$$

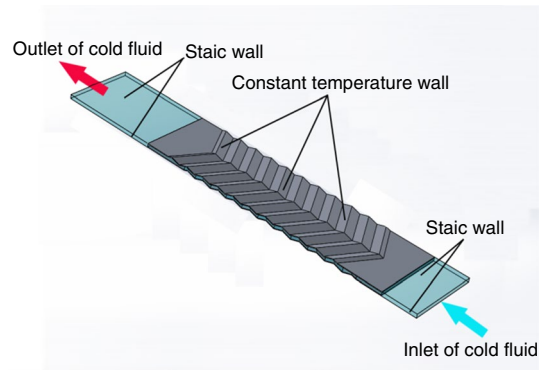


Fig. 3 Boundary condition instruction

Table 1 Values of structural parameters

Wavy plate dimensions	Values	Core dimensions	Values
Wavy plate length/mm	δ	Core width/mm	230
Wavy plate spacing/mm	λ	Core length/mm	60
Wavy plate angle/ $^\circ$	β		
Wavy plate thickness/mm	t		

$$\frac{\partial(\rho \epsilon)}{\partial t} + \frac{\partial(\rho k u_i)}{\partial x_i} = \frac{\partial}{\partial x_j} \left[\left(\mu + \frac{\mu_t}{\sigma_\epsilon} \right) \frac{\partial \epsilon}{\partial x_j} \right] + C_{1\epsilon} \frac{\epsilon}{k} (G_k + C_{3\epsilon} G_b) - C_{2\epsilon} \rho \frac{\epsilon^2}{k} + S_\epsilon \tag{6}$$

where the kinetic energy caused by the average velocity gradient:

$$G_k = \mu_t \left(\frac{\partial u_i}{\partial x_j} + \frac{\partial u_j}{\partial x_i} \right) \frac{\partial u_i}{\partial x_j} \tag{7}$$

The turbulent energy generated by the buoyancy effect G_b is:

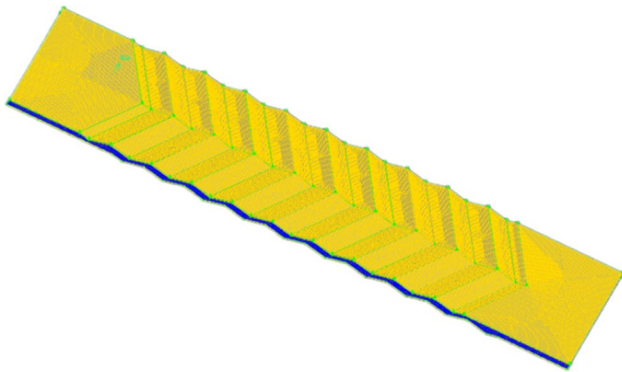
$$G_b = \beta g_i \frac{\mu_t}{Pr_t} \frac{\partial T}{\partial x_i} \tag{8}$$

The following values are used for standard $k-\epsilon$ model: $C_{1\epsilon} = 1.44$, $C_{2\epsilon} = 1.92$, $C_{3\epsilon} = 0.09$, $\sigma_k = 1.0$, $\sigma_\epsilon = 1.3$.

The single-channel geometry for numerical simulation is shown in detail in Fig. 3. And the structural parameters of plate is shown in Table 1. Considering the symmetry of the wavy plate structure, to bring down the time cost, the periodic boundary condition is used in simulation model. The inlet and outlet walls are set as adiabatic stationary walls. The inlet fluid velocity was 0.1 m s^{-1} , and the temperature was 50°C . The fin contact wall is set as thermostatic wall, and the temperature is 80°C . The outlet is set as a pressure outlet with standard atmospheric pressure (Table 1).

Table 2 Physical properties of fluid and solid [45]

	Coolant liquid	Air	Aluminum
Density/kg m ⁻³	1009.86	1.23	2719
Specific heat/J kg ⁻¹ °C ⁻¹	3679.4	1006.43	871
Thermal conductivity/W (m ⁻¹ °C ⁻¹)	0.643	0.024	237
Viscosity/Pa·s	7.13 × 10 ⁻⁴	0.011	–

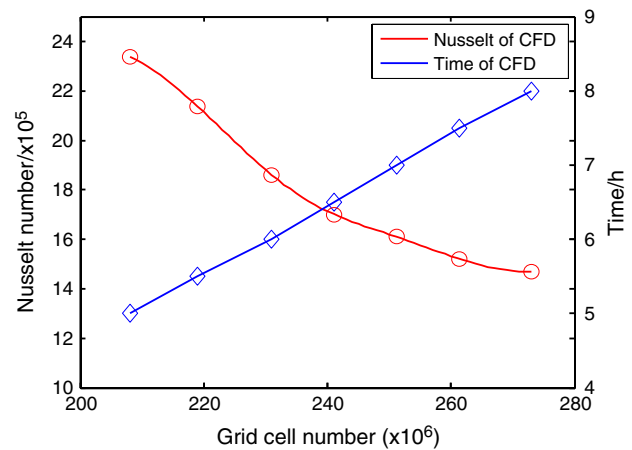
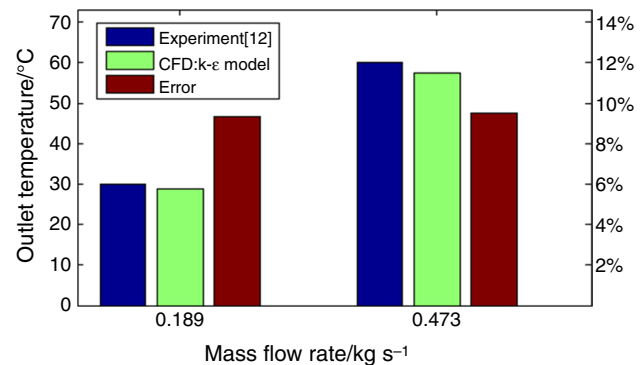
**Fig. 4** Grid for entire computational domain

Grid independence tests and verification of CFD model

ANSYS Fluent used finite volume method to solve the governing equation. This research selected the implicit solution based on pressure. Second-order MUSCL format is used for the convection term, velocity coupled with pressure is solved by SIMPLE algorithm. The physical properties of fluid and solid are given in Table 2.

This research used ANSYS mesh to discretize the solution domain. Hexahedral mesh partition is selected in order to obtain the simulation results with higher accuracy as shown in Fig. 4. In the CFD verification process, its independence was studied under seven different grid solutions, among which the number of meshes was 2.08 million, 2.19 million, 2.3 million, 2.39 million, 2.49 million, 2.61 million and 2.73 million. Because the Nusselt number is an important parameter for evaluating radiators, the optimal number of grids is comprehensively evaluated according to the Nusselt number and the time required for calculation. With the increase in the number of grids, the computing time is obviously extended, and the change of Nusselt number tends to be stable as shown in Fig. 5. Considering the accuracy of simulation and the cost of calculation, the number of grid cells is set at 2.39 million, which can meet the requirements of this study.

In order to verify the correctness of the above settings, CFD numerical solution was conducted according to the

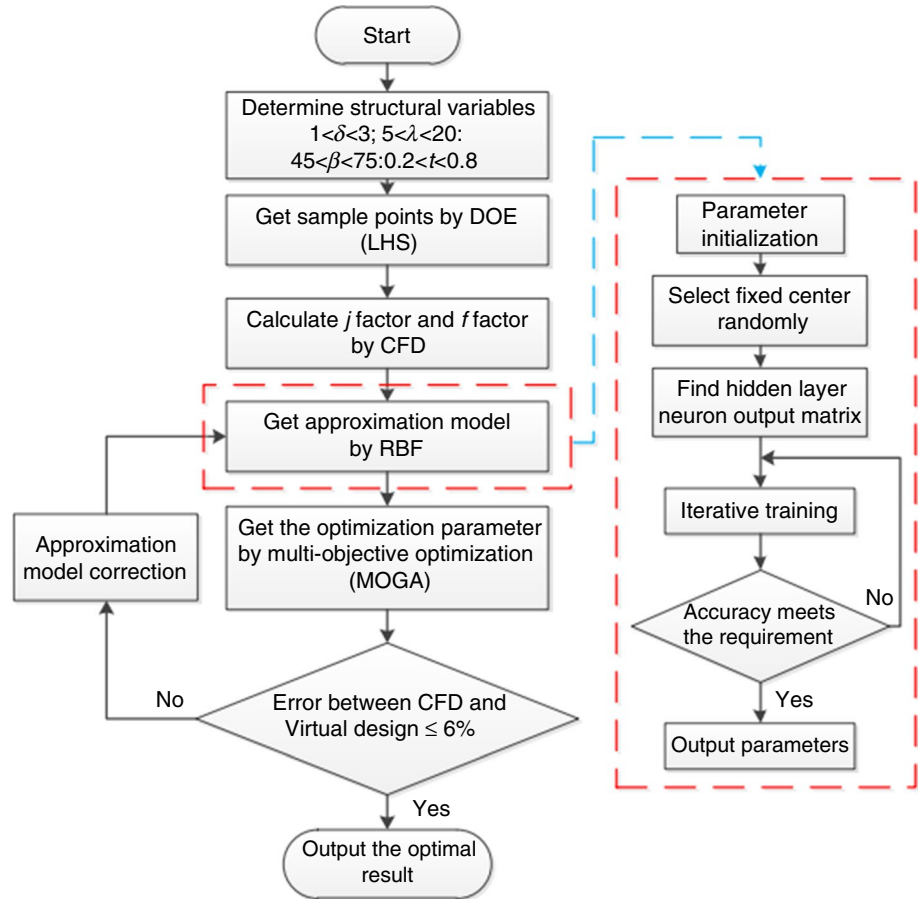
**Fig. 5** Grid independence verification**Fig. 6** Comparison of CFD result with experimental data [12]

A-type model parameters provided in literature [12]. The results were compared with experimental data as shown in Fig. 6. The error between simulation data and test data is not more than 10%, and the degree of coincidence is relatively high. The errors come from the iterative errors in the simulation model and the equipment errors in the test.

Optimal process of wavy plate heat exchangers

The multi-objective genetic algorithm (MOGA) is a typical method to search the optimal frontier of Pareto based on Pareto sequencing and niche technology to improve population diversity and prevent premature convergence of the solution group. In the process of MOGA calculation, an initial population is randomly generated and the objective function of each point is calculated. Based on Pareto's optimal concept, each individual in the population is sorted. This is done by associating each member of the group with the number of all other individuals in the

Fig. 7 Whole optimize process



group that govern the individual. The optimal solution is determined according to the constraint conditions. Sample points were established by using experimental design methods of Latin hypercube sampling (LHS). The whole optimize process is shown in Fig. 7.

• Step 1: Constraint condition

The shape optimization of plate heat exchangers is designed to achieve high heat transfer capability and low flow resistance. A large heat transfer factor j indicates a high heat exchange and relatively complex structure. The low friction factor f indicates that the channel is smooth and the resistance is small. And the structure is relatively simple. The heat transfer factor j and friction factor f is calculated by [48]:

$$\begin{cases} j = \frac{Nu}{Re Pr^{1/3}} \\ f = \frac{2\Delta PD}{\rho u^2 L} \end{cases} \quad (9)$$

Nu , Re and Pr are Nusselt number, Reynolds number and Prandtl number. They are defined as follows [47]:

$$\begin{cases} D = \frac{4S}{U} = \frac{4s(h-t)}{2[s+(h-t)]} = \frac{2s(h-t)}{s+h-2t} \\ Re = \frac{\rho Du}{\mu} \\ Pr = \frac{\mu c_p}{\lambda_t} \\ Nu = \frac{mc_p D(T_{out} - T_{in})}{\lambda_t S \Delta t_m} \end{cases} \quad (10)$$

The design parameters are wavy plate height δ , wavy plate spacing λ , wavy plate amplitude β and wavy plate thickness t . According to heat transfer factor j and friction factor f , the target function can be defined as follows:

$$F(X) = F(x_1, x_2, x_3, x_4) = F(\delta, \lambda, \beta, t) \quad (11)$$

According to the range of heat exchanger parameters [33], the wavy plate structure parameter is:

$$1 < \delta < 3, 5 < \lambda < 20, 45 < \beta < 75, 0.2 < t < 0.8. \quad (12)$$

This research chooses the largest heat transfer factor j and the smallest friction factor f as the optimized target function. They are defined as follows [48]:

$$\begin{aligned} \max j(x_i) &= \max F(\delta, \lambda, \beta, t) \\ \min f(x_i) &= \min F(\delta, \lambda, \beta, t) \end{aligned} \quad (13)$$

- Step 2: Structural parameter selection

Because of the nonlinear relationship between structural parameters and performance, LHS was used to obtain 50 groups of sample points to construct a three-dimensional model (parameters of the model listed in Table 5). Through the data of each sample point calculated by CFD, nonlinear relationship is further obtained, as shown in Fig. 13. Figure 13 shows the relationship between different structural characteristics, j and f .

- Step 3: Approximation model

Here, the RBF algorithm was applied to obtain the approximation model [48].

$$y = \sum_{i=1}^n w_{ij} \exp\left(-\frac{n}{2\sigma^2} \|x_p - c_i\|^2\right) \quad (14)$$

where w_{ij} is the mass of neurons between the hidden layer and the output layer, σ is the variance of basis function, n is the number of sample and c_i is the center of clustering.

The approximate relationship between design variable and objective function is determined by the above principles. Twenty control sample points are selected through Table 6. And the availability of the approximate model was determined by comparing the CFD values of these points with the budget values of the approximate model. RMSE was chosen as the criterion for approximate model availability and the equation is shown in Eq. 7 [48].

$$\text{RMSE} = \sqrt{\left[\frac{\sum_{i=1}^n (X_{\text{CFD}} - X_{\text{model}})^2}{n} \right]} \quad (15)$$

The results showed that $\text{RMSE } j=0.093$ and $\text{RMSE } f=0.171$. The error is lower than the engineering application requirement.

- Step 4: Multi-objective optimization

MOGA is used to solve the optimal solution in the approximate model and set the maximum value of j/f as the target function.

Optimal results

According to the above procedure, the maximum value of j/f is obtained and the corresponding optimized structure parameters of $\delta, \lambda, \beta, t$ are shown in Table 3. Table 4 shows

Table 3 Structural parameters before and after optimization

	Δ/mm	Λ/mm	$\beta/^\circ$	t/mm
Before optimization	2.3	10	60	0.6
After optimization	2.87	16.67	63.85	0.49

Table 4 Comparison between the CFD and approximation

	Heat transfer factor j	Friction factor f
CFD	1.8×10^{-6}	0.014
Approximation	1.7×10^{-6}	0.013
Error	5.88%	7.14%

the results of j and f , respectively, calculated by approximate model and CFD optimization under corresponding optimization results. The comparison results show that the error of j and f of the approximate model is less than 8%, which verifies the reliability of the approximate model again. The benchmark solution was chosen as the before optimization [12].

Figure 13 shows that nonlinear relationship between parameters and performances. The wavy plate angle has the most obvious effect on j , and that of wave plate angle is the weakest. At The same time, the wavy plate angle has strongest effect on f , while the wavy plate spacing has almost no effect on f .

Figure 8 shows the CFD cloud diagram of the longitudinal section of the flow rate, temperature and pressure between the optimized structure and the original structure.

It can be seen from the figures that the fluid flowing through the plate generates strong turbulent movement in the groove accompanied by obvious heat transfer. The bulge on the plate is a place with a higher velocity gradient. Because of the presence of the convex structure, the fluid impinges on the convex structure to thin the near-wall flow layer and reduce the thermal resistance. There is the fluid turbulence phenomenon at the raised intersection point. The turbulence is good to heat transfer.

In general, the cloud map distribution of each field is basically the same before and after optimization. Fluid flow between plates is very uneven from the flow form. Compared with the average value of each field, the velocity increases 0.01%. The pressure field was decreased by 40%, and the temperature was decreased by 2.5%. With the increase in the wave height, the flow form by cross-flow gradually becomes tortuous flow. At this point, the contact has a great impact on the flow of the fluid. The contact has a strong disturbance effect on the flow, making the heat exchange between the fluid and the solid wall surface and between the fluid and the fluid more intense, and the temperature rise decreases with the increase in the wave

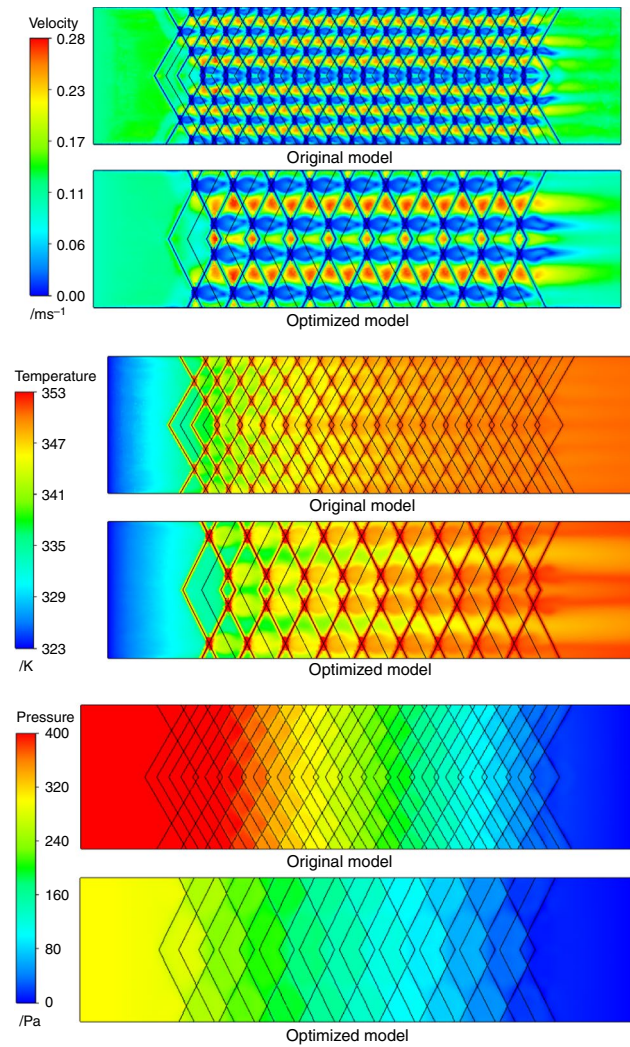


Fig. 8 Flow field comparison between the optimized model and the original model

distance. Because of the resistance of the contact to the fluid, the low-speed vortex area is formed after the contact. The optimized fluid velocity is gentle, the pressure is small, the temperature distribution is more uniform, and the heat dissipation effect is more obvious.

To sum up, although the equivalent diameter of optimized structure increases, the fluid friction resistance decreases and the heat transfer capacity increases. The optimized wavy plate heat exchanger is improved.

The field synergy analysis

As we all known, in conduction and convection problems, the presence of heat sources leads to an increase in heat flux at the boundary. So, the heat transfer capacity is

demonstrated not only by the velocity vector and the temperature gradient, but also by their synergy.

The field synergy theory indicates that the synergetic between velocity vector and temperature gradient is better, and the heat transfer capacity is higher. In this research, the field synergy principle is introduced to evaluate the wavy plate. The relationship between the physical fields is shown in Fig. 9. The field synergy quantity is defined as follows [46]:

$$\begin{cases} \beta = \arccos \frac{U \nabla T}{|U| |\nabla T|} \\ \theta = \arccos \frac{U \nabla p}{|U| |\nabla p|} \\ \gamma = \arccos \frac{\nabla T \nabla u}{|\nabla T| |\nabla u|} \end{cases} \quad (16)$$

Field synergy angle α

The field synergy angle α is the angle between velocity vector and temperature gradient. The comparison of field synergy angle α between the original and optimized model is shown in Fig. 10. Combined with the heat transfer principle, the coolant flows to the right direction along the plate. Meanwhile, the plate continuously transfers heat flux by convection and its direction is perpendicular to the plate, so the velocity direction tends to be perpendicular to the temperature gradient. Moreover, the heat transfer capacity increases with the synergy angle decrease at the bending point of the plate. All in all, the optimized model achieved smaller α and better heat transfer capacity.

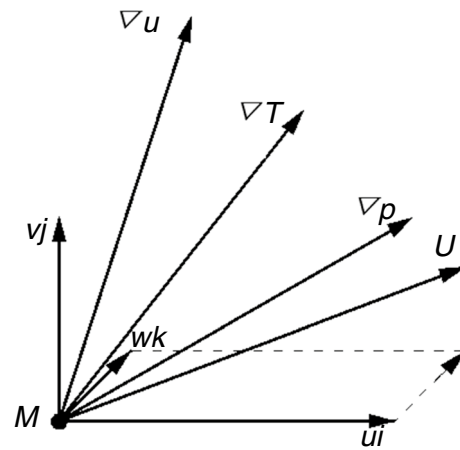


Fig. 9 Relationships between the physical fields

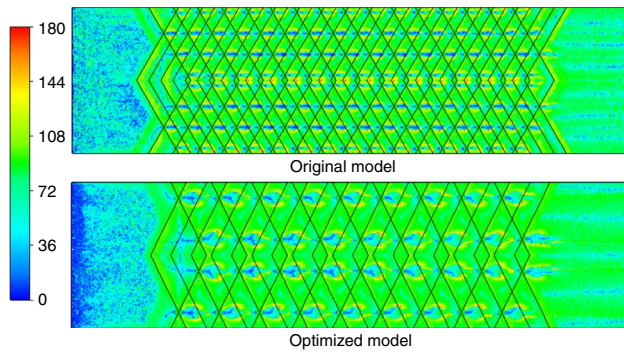


Fig. 10 Comparison of synergy angle α

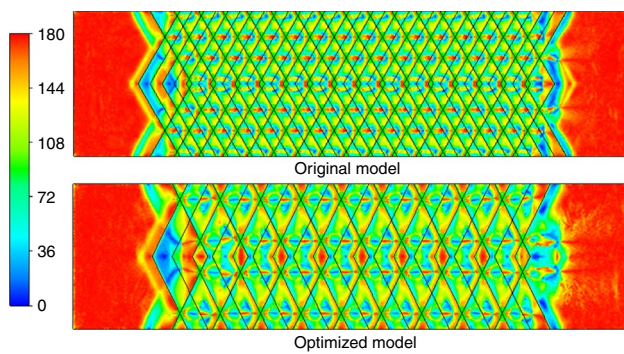
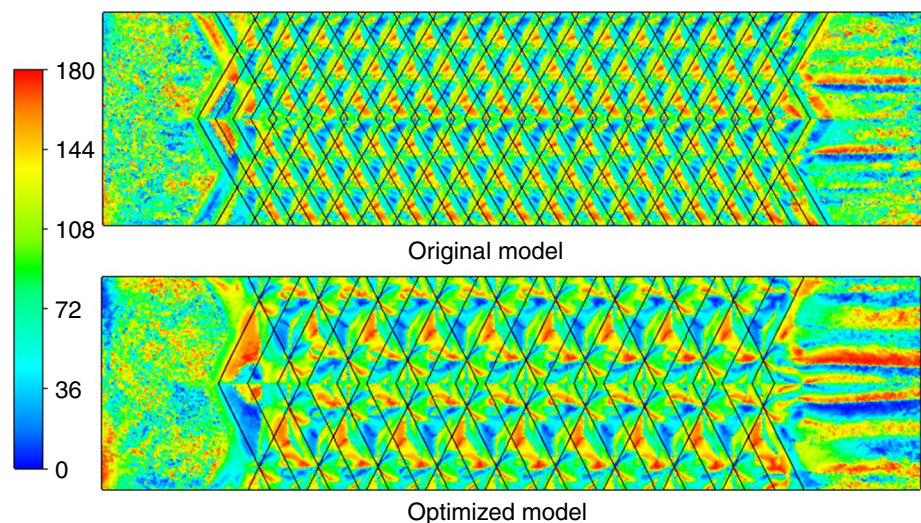


Fig. 11 Comparison of synergy angle θ

Fig. 12 Comparison of synergy angle γ



Synergy angle θ

The synergy angle θ between velocity and pressure gradient represents flow resistance, as shown in Fig. 11. The synergy angle of the two models is relatively similar. At the bend, the fin blocks the flow of coolant, resulting in a deviation between the near-wall flow and main flow direction. Then the θ is larger and the flow resistance is increased accordingly. In reality, elsewhere, it is clear that the θ of the optimized model is smaller than that of the original model. Combined with the pressure distribution in the flow field, it can be known that although the pressure drop in the optimized model is larger, a reasonable structure parameter can reduce the friction coefficient f .

Synergy angle γ

A comparison of synergy angle γ which characterizes convection intensity and drag reduce, is shown in Fig. 12. As is known, a larger γ indicates a better overall heat transfer capacity. So, the performance improvement is shown through a relatively large γ obtained by the optimization model. It was also found that the γ near the bend of the fin was larger than the other locations in plate, indicating that major heat transfer was taking place here.

Overall, the optimization model has relatively small angle of β and θ indicate more efficient heat transfer. At the same time, larger γ values are also decided as better heat transfer capacity. The heat transfer mechanism of plate heat exchanger can be better understood by the field coordination theory, which provides a reasonable basis for the structural design.

Conclusions

In this research, the plate heat exchanger was chosen as research object and the plate structure was optimized by RBF and MOGA. The optimized structure reduced the coolant temperature by 2.5% and the pressure drop by 40%. The speed of optimization has also improved significantly. In general, the optimized heat transfer rate of corrugated plate can fully meet the performance requirements of heat exchanger, and the field

synergy number is analyzed. We will combine the heat transfer performance of heat exchanger with the economic efficiency of processing to optimize the design, in the future study.

Appendix

See Tables 5 and 6, Fig. 13.

Table 5 50 sets of structural parameters sample points

Num	δ/mm	λ/mm	$\beta/^\circ$	t/mm	Num	δ/mm	λ/mm	$\beta/^\circ$	t/mm
1	2.26	18.18	64.38	0.46	26	1.82	10.98	54.08	0.72
2	2.58	17.16	46.62	0.74	27	1.96	13.06	68.16	0.56
3	1.86	13.26	70.6	0.42	28	2.46	19.8	51.74	0.44
4	2.32	15.56	45.32	0.34	29	2.22	8.8	47.64	0.32
5	2.36	10.24	59.82	0.52	30	2.94	18.86	60.94	0.72
6	1.22	12.08	47.2	0.44	31	2.06	16.7	72.76	0.24
7	1.12	9.7	55.9	0.76	32	3	6.12	62.58	0.4
8	1.62	8.12	48.08	0.64	33	2.02	7.26	53.18	0.66
9	1.42	15.32	66.6	0.68	34	2.7	19.24	61.96	0.66
10	2.16	10.1	56.5	0.6	35	1.76	7.98	51.5	0.26
11	2.8	10.42	50.42	0.38	36	2.74	14.18	46.18	0.7
12	2.3	9.16	65.74	0.2	37	1.6	14.78	50.24	0.28
13	1.26	19.68	57.52	0.26	38	1.04	7.66	71	0.3
14	2.5	13.64	67.6	0.58	39	2.42	5.24	53.76	0.32
15	2.68	14.32	71.52	0.78	40	1.9	15.08	58.86	0.48
16	2.12	17.38	63.22	0.34	41	1.04	18.56	49.74	0.22
17	1.66	15.9	68.68	0.76	42	1.12	17.68	49.12	0.56
18	2.6	8.5	67.18	0.8	43	1.7	5.86	55.7	0.5
19	2.84	11.04	57.7	0.54	44	1.96	9.2	58.36	0.38
20	1.54	16.32	60.52	0.28	45	2.56	6.94	69.96	0.68
21	2.84	6.24	61.58	0.6	46	1.48	12.26	73.22	0.5
22	1.3	5.5	74.02	0.22	47	1.34	11.6	69.26	0.64
23	1.6	13.84	72.12	0.72	48	1.78	18.42	52.38	0.58
24	2.88	16.64	63.86	0.52	49	1.36	6.66	74.5	0.36
25	2.16	11.82	54.88	0.46	50	1.46	12.64	64.9	0.46

Table 6 20 sets of contrast sample points

Num	δ/mm	λ/mm	$\beta/^\circ$	t/mm	Num	δ/mm	λ/mm	$\beta/^\circ$	t/mm
1	1	10	55	0.4	10	2	10	45	0.4
2	1.5	10	55	0.4	11	2	10	55	0.4
3	2	10	55	0.4	12	2	10	65	0.4
4	2.5	10	55	0.4	13	2	10	75	0.4
5	3	10	55	0.4	14	2	10	55	0.4
6	2	5	55	0.4	15	2	10	55	0.2
7	2	10	55	0.4	16	2	10	55	0.4
8	2	15	55	0.4	17	2	10	55	0.6
9	2	20	55	0.4	18	2	10	55	0.8

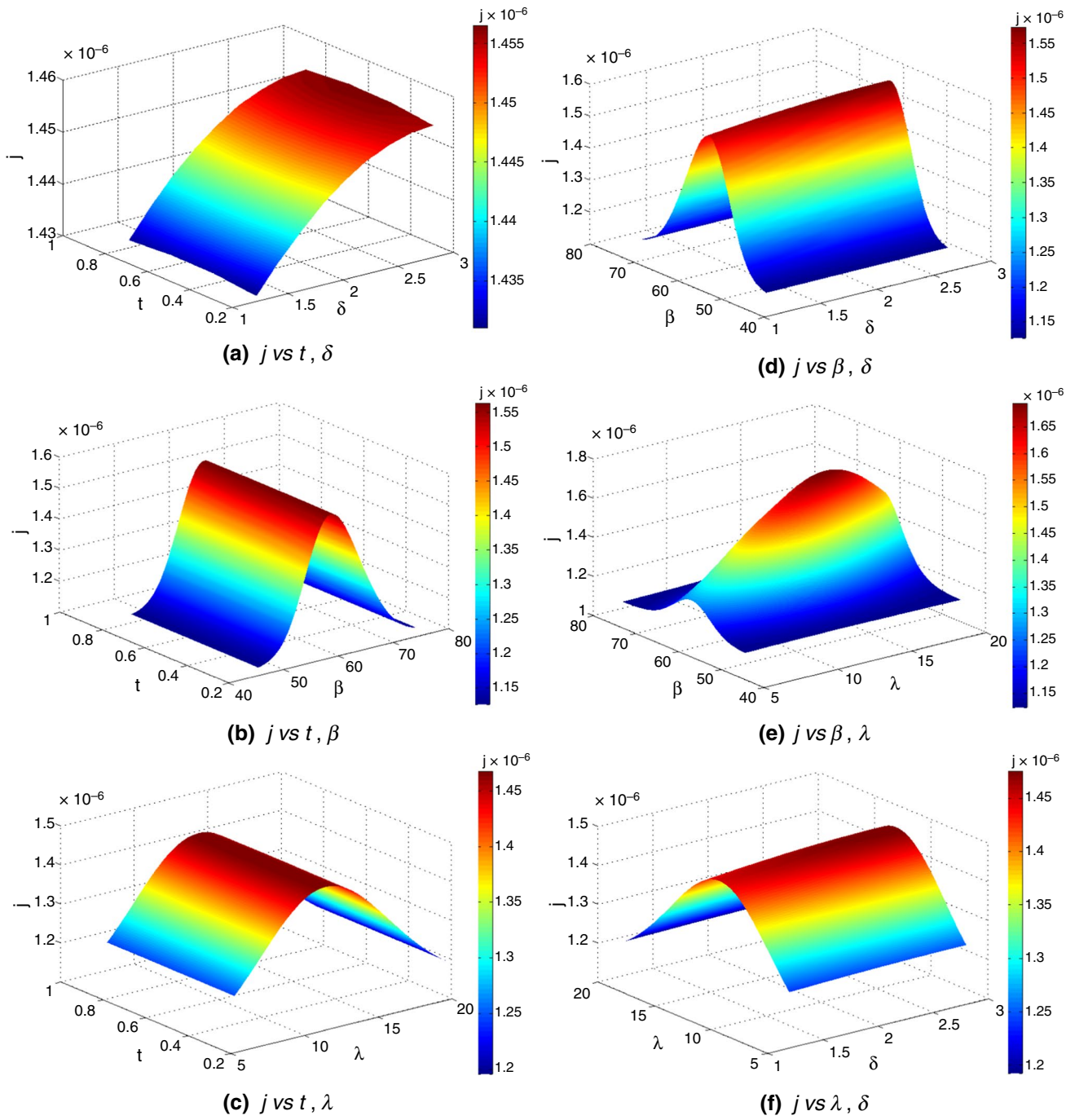


Fig. 13 Nonlinear relationship between parameters and performances. **a** j vs t, δ . **b** j vs t, β . **c** j vs t, λ . **d** j vs β, δ . **e** j vs β, λ . **f** j vs λ, δ . **g** f vs t, δ . **h** f vs t, β . **i** f vs t, λ . **j** f vs β, δ . **k** f vs β, λ . **l** f vs λ, δ .

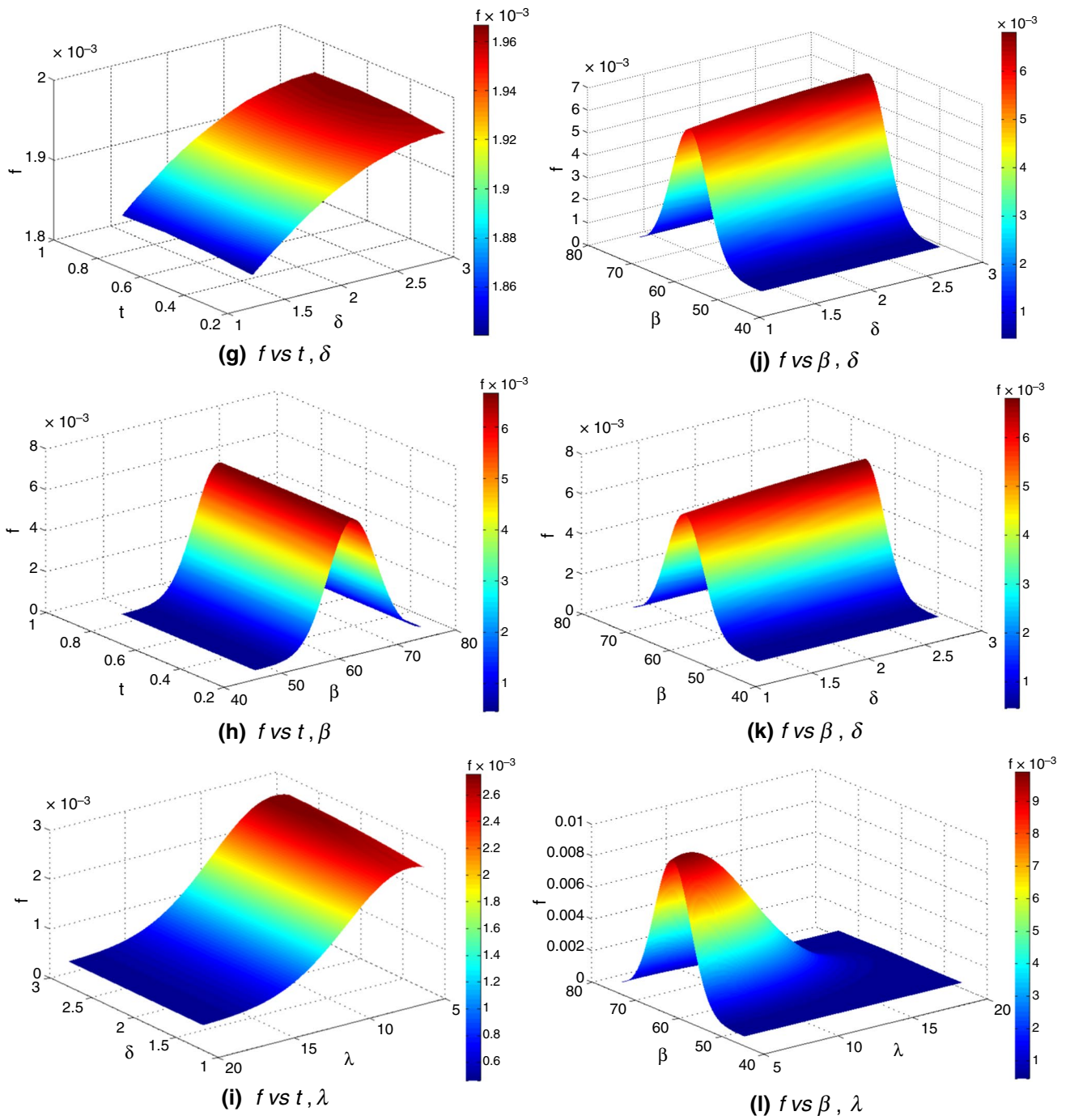


Fig. 13 (continued)

References

- Raja BD, Jhala RL, Patel V. Thermal-hydraulic optimization of plate heat exchanger: a multi-objective approach[J]. *Int J Therm Sci.* 2018;124:522–35.
- Embaye M, Al-Dadah RK, Mahmoud S. Numerical evaluation of indoor thermal comfort and energy saving by operating the heating panel radiator at different flow strategies[J]. *Energy Build.* 2016;121:298–308.
- Tao C, Jie W, Wei P. Flow and heat transfer analyses of a plate-fin heat exchanger in an HTGR[J]. *Annals Nuclear Energy.* 2017;108:871.
- Samadifar M, Toghraie D. Numerical simulation of heat transfer enhancement in a plate-fin heat exchanger using a new type of vortex generators[J]. *Appl Thermal Eng.* 2018;133:87.
- Jin S, Hrnjak P. Effect of end plates on heat transfer of plate heat exchanger[J]. *Int J Heat Mass Transf.* 2017;108:740–8.
- Grabenstein V, Polzin AE, Kabelac S. Experimental investigation of the flow pattern, pressure drop and void fraction of two-phase flow in the corrugated gap of a plate heat exchanger[J]. *Int J Multiph Flow.* 2017;91:155–69.
- Shenghan J, Pega H. A new method to simultaneously measure local heat transfer and visualize flow boiling in plate heat exchanger[J]. *Int J Heat Mass Transf.* 2017;113:45.
- Xuan T, Nuijten MP, Infante CA. Two-phase vertical downward flow in plate heat exchangers: Flow patterns and condensation mechanisms[J]. *Int J Refrigeration.* 2018;85:41.
- Junqi D, Xianhui Z, Jianzhang W. Experimental study on thermal hydraulic performance of plate-type heat exchanger applied in engine waste heat recovery[J]. *Arab J Sci Eng.* 2018;43(3):1153–63.
- AminHossein J, Enzo Z. Effects of position and temperature-gradient direction on the performance of a thin plane radiator[J]. *Appl Thermal Eng.* 2016;105:87.
- Bhattad A, Sarkar J, Ghosh P. Discrete phase numerical model and experimental study of hybrid nanofluid heat transfer and pressure drop in plate heat exchanger[J]. *Int Commun Heat Mass Transfer.* 2018;91:262–73.
- Dutta OY, Rao BN. Investigations on the performance of chevron type plate heat exchangers[J]. *Heat Mass Transf.* 2018;54(3):1–13.
- Lowrey S, Sun Z. Experimental investigation and numerical modelling of a compact wet air-to-air plate heat exchanger[J]. *Appl Therm Eng.* 2017;131:89–101.
- Kumar B, Singh SN. Study of pressure drop in single pass U-type plate heat exchanger[J]. *Exper Thermal Fluid Sci.* 2017;4:7717301310.
- Jiang Q, Zhuang M, Zhang Q, et al. Experimental study on the thermal hydraulic performance of plate-fin heat exchangers for cryogenic applications[J]. *Cryogenics.* 2018;65:17303715.
- Hong SW, Duong XQ, Chung JD. Reassessment on the application of the embossed plate heat exchanger to adsorption chiller[J]. *J Mech Sci Technol.* 2018;32(3):1431–6.
- Kunpeng G, Nan Z, Robin S. Design optimisation of multi-stream plate fin heat exchangers with multiple fin types[J]. *Appl Thermal Eng.* 2018;131:787.
- Li R, Liu J, Xiongwen X. Development and validation of a direct passage arrangement method for multistream plate fin heat exchangers[J]. *Appl Thermal Eng.* 2018;130:51.
- Raja BD, Jhala RL, Patel V. Multiobjective thermo-economic and thermodynamics optimization of a plate-fin heat exchanger: RAJA et al[J]. *Heat Transfer–Asian Res.* 2018;47(9):80.
- Liu JC, Wei XT, Zhou ZY. Numerical analysis on interactions between fluid flow and structure deformation in plate-fin heat exchanger by Galerkin method[J]. *Heat Mass Transfer.* 2018;2018:1–10.
- Chennu R. Numerical analysis of compact plate-fin heat exchangers for aerospace applications[J]. *Int J Numer Meth Heat Fluid Flow.* 2018;28(6):00–00.
- Zhang Q, Xu L, Li J. Performance prediction of plate-fin radiator for low temperature preheating system of proton exchange membrane fuel cells using CFD simulation[J]. *Int J Hydrogen Energy.* 2017;2017:19917331208.
- Al-Obaidi AR. Investigation of fluid field analysis, characteristics of pressure drop and improvement of heat transfer in three-dimensional circular corrugated pipes[J]. *J Energy Storage.* 2019;26:1010121–10101221.
- Al-Obaidi AR, Alhamid J. Numerical investigation of fluid flow, characteristics of thermal performance and enhancement of heat transfer of corrugated pipes with various configurations[J]. *J Phys: Conf Ser.* 2021;1733: 012004.
- Al-Obaidi AR. Study the influence of concavity shapes on augmentation of heat-transfer performance, pressure field, and fluid pattern in three-dimensional pipe[J]. *Heat Transfer.* 2021;8:87.
- Al-Obaidi AR. Investigation of the flow, pressure drop characteristics, and augmentation of heat performance in a 3D flow pipe based on different inserts of twisted tape configurations[J]. *Heat Transfer.* 2021;50:5049.
- Al-Obaidi AR, Sharif A. Investigation of the three-dimensional structure, pressure drop, and heat transfer characteristics of the thermohydraulic flow in a circular pipe with different twisted-tape geometrical configurations[J]. *J Thermal Anal Calorimetry.* 2020;143:1–26.
- Al-Obaidi AR. Analysis of the flow field, thermal performance, and heat transfer augmentation in circular tube using different dimple geometrical configurations with internal twisted-tape insert[J]. *Heat Transfer.* 2020;49(8):4153–72.
- Al-Obaidi AR. Investigation of the flow, pressure drop characteristics, and augmentation of heat performance in a 3D flow pipe based on different inserts of twisted tape configurations[J]. *Heat Transfer.* 2021;50(5):5049–79.
- Al-Obaidi AR, Chaer I. Study of the flow characteristics, pressure drop and augmentation of heat performance in a horizontal pipe with and without twisted tape inserts[J]. *Case Stud Therm Eng.* 2021;25(10): 100964.
- Alhamid J, Al-Obaidi AR. Effect of concavity configuration parameters on hydrodynamic and thermal performance in 3D circular pipe using Al₂O₃ nanofluid based on CFD simulation. *J Phys: Conf Ser.* 2021;1845(1): 012060.
- Zhicheng Y, Lijun W, Zhaokuo Y. Shape optimization of welded plate heat exchangers based on grey correlation theory[J]. *Appl Thermal Eng.* 2017;123:1282.
- Shon BH, Jung CW, Kwon OJ. Characteristics on condensation heat transfer and pressure drop for a low GWP refrigerant in brazed plate heat exchanger[J]. *Int J Heat Mass Transf.* 2018;122:1272–82.
- Wen J, Li K, Zhang X. Optimization investigation on configuration parameters of serrated fin in plate-fin heat exchanger based on fluid structure interaction analysis[J]. *Int J Heat Mass Transfer.* 2018;119:282.
- Faizan M, Ahmed R, Ali HM. A critical review on thermophysical and electrochemical properties of Ionanofluids (nanoparticles dispersed in ionic liquids) and their applications[J]. *J Taiwan Inst Chem Eng.* 2021;124:391.
- Chamkouri H, Ahmadlouydarab M, Talebi H, et al. Excellent electromagnetic wave absorption by complex systems through hybrid polymerized material[J]. *Polymer Bull.* 2021;31:955.
- Vasconcelos Segundo EHD, Amoroso AL, Mariani VC. Thermodynamic optimization design for plate-fin heat exchangers by Tsallis JADE[J]. *Int J Thermal Sci.* 2017;113:136–44.
- Turgut MS, Turgut OE. Ensemble shuffled population algorithm for multi-objective thermal design optimization of a plate frame

- heat exchanger operated with Al₂O₃/water nanofluid [J]. *Appl Soft Comput.* 2018;69:250–69.
39. Jian W, Yanzhong L, Huihu Y. A mathematical model for flow maldistribution study in a parallel plate-fin heat exchanger[J]. *Appl Thermal Eng.* 2017;121:462.
 40. Shah Z, Sheikholeslami M, Kumam P. CFD simulation of water-based hybrid nanofluid inside a porous enclosure employing Lorentz forces[J]. *IEEE Access.* 2019;7:99.
 41. Sheikholeslami M, Shah Z, Shafee A. Uniform magnetic force impact on water based nanofluid thermal behavior in a porous enclosure with ellipse shaped obstacle[J]. *Scientif Rep.* 2019;9(1):41.
 42. Shutaywi M, Shah Z. Mathematical modeling and numerical simulation for nanofluid flow with entropy optimization[J]. *Case Stud Thermal Eng.* 2021;6: 101198.
 43. Ahmad S, Ali K, Rizwan M. Heat and mass transfer attributes of copper-aluminum oxide hybrid nanoparticles flow through a porous medium[J]. *Case Stud Thermal Eng.* 2021;25: 100932.
 44. Ramezanizadeh M, Alhuyi Nazari M, Ahmadi MH. Experimental and numerical analysis of a nanofluidic thermosyphon heat exchanger[J]. *Eng Appl Comput Fluid Mech.* 2019;13(1):40–7.
 45. Assad M, Nazari MA. Heat exchangers and nanofluids[j] design and performance optimization of renewable energy systems. Elsevier; 2021.
 46. Yu C, Xue X, Shi K, Shao M, Liu Y. Comparative study on CFD turbulence models for the flow field in air cooled radiator. *Processes.* 2020;8(12):1687.
 47. Khan A, Ali HM, Nazir R. Experimental investigation of enhanced heat transfer of a car radiator using ZnO nanoparticles in H₂O–ethylene glycol mixture[J]. *J Therm Anal Calorim.* 2019;6:1–15.
 48. Yu C, Xue X, Shi K, Shao M. A three-dimensional numerical and multi-objective optimal design of wavy plate-fins heat exchangers. *Processes[J].* 2021;9:91.
- Publisher's Note** Springer Nature remains neutral with regard to jurisdictional claims in published maps and institutional affiliations.